Excitation and control of large-amplitude standing magnetization waves

L. Friedland* and A. G. Shagalov†
Racah Institute of Physics, Hebrew University of Jerusalem, Jerusalem 91904, Israel;
Institute of Metal Physics, Ekaterinburg 620990, Russian Federation;
and Ural Federal University, Mira 19, Ekaterinburg 620002, Russian Federation

(Received 23 July 2018; revised manuscript received 29 October 2018; published 10 January 2019)

A robust approach to excitation and control of large amplitude standing magnetization waves in an easy axis ferromagnetic by starting from a ground state and passage through resonances with chirped frequency microwave or similar alternative drives (spin torque, additional periodic anisotropy) is proposed. The formation of these waves involves two stages, where in the first stage, a spatially uniform, precessing magnetization is created via passage through a resonance followed by a self-phase-locking (autoresonance) with a constant amplitude drive. In the second stage, the passage through an additional resonance with a spatial modulation of the driving amplitude yields transformation of the uniform solution into a doubly phase-locked standing wave, whose amplitude is controlled by the variation of the driving frequency. The stability of this excitation process is analyzed both numerically and via Whitham's averaged variational principle.

DOI: 10.1103/PhysRevB.99.014411

I. INTRODUCTION

Because of the complexity and despite decades of studies, magnetization dynamics in ferromagnetic materials remains of interest to basic and applied research. For example, nonlinear spin waves and solitons in ferromagnetic films were studied experimentally extensively (e.g., Refs. [1–4]). Magnetostatic and boundary effects in such macroscopic films yield complex dispersion of the spin waves. Depending on the sign of the dispersion both bright and dark magnetic solitons were observed. The long wavelength approximation in this problem yields the nonlinear Schrodinger (NLS) model, providing a convenient theoretical basis for investigation. The NLS equation has well known traveling wave and soliton solutions [5], allowing interpretation of the experimentally observed magnetization dynamics.

In recent years, applications in ferromagnetic nanowires opened new perspectives in studying magnetization waveforms [6]. At the nanoscales a quasi-one-dimensional symmetry can be realized and magnetostatic effects can be reduced to additional contributions to the anisotropy [6–8], which can be conveniently modeled by the Landau-Lifshitz-Gilbert (LLG) equation. It is known that the one-dimensional (1D), dissipationless LLG equation, similar to the NLS equation, is integrable and has a multitude of exact solutions including solitons and spatially periodic waveforms [6,9,10], expected to be observed in nanowires. The simplest solitons are domain walls, which are studied extensively [11–15] as a basis for new memory and logic devices [16,17]. A different type of solitons are so-called breathers [6], which can be interpreted as an interacting pair of domain walls with opposite topological charges (soliton-antisoliton pair). They are stable localized objects in easy-axis ferromagnetic when dissipation is negligible [9], which was also illustrated in numerical simulations [18]. These breather solitons correspond to the bright NLS solitons in the small amplitude approximation [9]. Solitons in ferromagnetic nanowires with a spin polarized current were also discussed in Refs. [19,20] in the framework of a modified NLS model.

In this paper, we focus on excitation of large amplitude standing LLG waves in an easy axis ferromagnetic, such that the projection M_z of the magnetization vector $\mathbf{M}$ on the easy axis is independent of time and periodic in z, while $\mathbf{M}_\perp$ precesses uniformly around the axis. These waves approach a soliton limit as their wavelength increases (see below). The question is how to generate such waves by starting from a *simple* initial equilibrium and how to control their dynamics. Excitation by an impulse or localized external fields usually are unsuitable for generating pure large amplitude standing waves because of significant residual perturbations. Here, we suggest a simple method of exciting these waves based on the autoresonance approach via driving the system by a small, chirped frequency external rotating magnetic field or similar alternative drives. This approach allows us to excite the waves with a predefined amplitude and phase and stabilize them with respect to dissipation. The autoresonance approach uses the salient property of a nonlinear system to stay in resonance with driving perturbations despite slow variation of parameters. The idea was used in many applications starting from particle accelerators [21,22], through planetary dynamics [23], [24] and atomic physics [25,26], to plasmas [27], magnetization dynamics in single domain nanoparticles [28–30], and more. Autoresonant excitation of both bright and dark solitons and spatially periodic multiphase waves within the NLS model were studied in Ref. [31–33], while the autoresonant control of NLS solitons is described in Refs. [34,35]. In all these applications, one drives the system of interest by an oscillating perturbation, captures it into a nonlinear

*lazar@mail.huji.ac.il
†shagalov@imp.uran.ru

resonance, while slowly varying the driving frequency (or other parameter). The resulting continuing self-phase-locking (autoresonance) yields excursion of the system in its solutions space, frequently leading to emergence and control of nontrivial solutions. In this work, motivated by the aforementioned results in related driven-chirped NLS systems, we apply a similar approach yielding arbitrary amplitude, standing magnetization waves.

The scope of the presentation will be as follows. In Sec. II, we introduce our autoresonant magnetization model and discuss the problem of capturing the system into resonance with a chirped frequency microwave field followed by formation of an autoresonant, spatially uniform magnetization state. In Sec. III, we study transition from the uniform state to a standing wave by spatially modulating the amplitude of the chirped frequency drive. In the same section, we will illustrate this process in simulations and present a qualitative picture of the dynamics. Section IV will be focused on the theory of the autoresonant standing waves and discuss their modulational stability via Whitham's averaged variational principle [36]. In Sec. V, we illustrate excitation of the standing waves via two alternative driving mechanisms involving spin torque or the addition of spatially modulated hard axis anisotropy. Finally, Sec. VI will present our conclusions.

II. AUTORESONANT MAGNETIZATION MODEL

Our starting point is the $1D$ Landau-Lifshitz-Gilbert (LLG) equation for a ferromagnetic with the easy axis along $\widehat{\mathbf{e}}_z$ in an external magnetic field $\mathbf{H} = H_0\widehat{\mathbf{e}}_z$ and in the presence of a weak rotating driving microwave field $\mathbf{H}_d = b\cos(\cos\varphi_d\widehat{\mathbf{e}}_x + \sin\varphi_d\widehat{\mathbf{e}}_y)$ having spatially periodic amplitude $b = b_0 + b_1\cos(kz)$ ($k = 2\pi/L$, L being periodicity length) and slowly chirped frequency $\omega_d(t) = -\partial\varphi_d/\partial t$:

$$\frac{\partial\mathbf{m}}{\partial\tau} = \mathbf{h}\times\mathbf{m} + \lambda\mathbf{m}\times\frac{\partial\mathbf{m}}{\partial\tau}. \tag{1}$$

Here λ is the Gilbert damping parameter,

$$\mathbf{h} = \frac{\partial^2\mathbf{m}}{\partial\xi^2} + (m_z + h_0)\widehat{\mathbf{e}}_z + \varepsilon(\cos\varphi_d\widehat{\mathbf{e}}_x + \sin\varphi_d\widehat{\mathbf{e}}_y), \tag{2}$$

and we use normalized magnetization $\mathbf{m} = \mathbf{M}/M$, dimensionless time $\tau = (\gamma K/M)t$, and coordinate $\xi = z/\delta$, $\delta = \sqrt{A/K}$ (γ, A, and K being the gyromagnetic ratio, the exchange constant, and the anisotropy constant, respectively). Furthermore in Eq. (2), $h_0 = MH_0/K$, $\varepsilon = \varepsilon_0 + \varepsilon_1\cos(\kappa\xi)$, $\varepsilon_{0,1} = Mb_{0,1}/K$, $\varphi_d = -\int\Omega_d d\tau$, $\Omega_d(\tau) = \omega_d M/(K\gamma)$, $\kappa = 2\pi/l$, and $l = L/\delta$.

The proposed approach to excitation of magnetization waves requires realization of the proper driving field. For example, consider the Permalloy parameters $A = 10^{-11}$ J/m, $K = 10^5$ J/m^3, and $M = 8\times10^5$ A/m [15]. This yields the characteristic width $\delta = 10$ nm, the linear resonance frequency (see below) $f_0 = \gamma K/(2\pi M)(1 + h_0) = 3.5(1 + h_0)$ GHz, and the driving magnetic field amplitude $b_0 = \varepsilon_0 K/M = 3.75\times10^{-4}$ T for $\varepsilon_0 = 0.003$ (as in examples in Fig. 3 below). The periodicity length L in our driven problem is $l\delta$. We will use $l \sim 10$ in the examples below, which corresponds to $L \sim 100$ nm. Spatial modulation of the microwave magnetic field on this submicron scale is difficult. However, analogous autoresonant excitations of the magnetization wave can be obtained by introducing other components in the effective magnetic field $\mathbf{h}$ of a similar form but due to different physical effects. Two such alternatives will be discussed in Sec. V.

We seek spatially periodic solutions of Eq. (1) and proceed from the dissipationless version of this equation in polar coordinates ($m_x = \sin\theta\cos\varphi$, $m_y = \sin\theta\sin\varphi$, $m_z = \cos\theta$):

$$\theta_\tau = \Phi_{\xi\xi}\sin\theta + 2\Phi_\xi\theta_\xi\cos\theta - \varepsilon\sin\Phi, \tag{3}$$

$$\Phi_\tau = \left(-\frac{1}{\sin\theta}\theta_{\xi\xi} + \Phi_\xi^2\cos\theta\right) + \cos\theta - \Omega_d'(\tau) - \varepsilon\cot\theta\cos\Phi, \tag{4}$$

where $\Phi = \varphi - \varphi_d$ is the phase mismatch and $\Omega_d' = \Omega_d - h_0$. This system is a spatial generalization of the recently studied autoresonant magnetization switching problem in single-domain nanoparticles [28,29], where one neglects the spatial modulation of the driving amplitude (so $\varepsilon = \varepsilon_0$) and the spatial derivatives in Eqs. (3) and (4) to get

$$\theta_\tau = -\varepsilon\sin\Phi, \tag{5}$$

$$\Phi_\tau = \cos\theta - \Omega_d'(\tau) - \varepsilon\cot\theta\cos\Phi. \tag{6}$$

In the 1D ferromagnetic case, Eqs. (5) and (6) describe a spatially uniform, rotating around the axis magnetization dynamics. In the rest of this section, we discuss formation and stability of autoresonant uniform states in the dissipationless case but include dissipation in numerical simulations for comparison.

The autoresonance idea is based on a self-sustained phase locking of the driven nonlinear system to chirped frequency driving perturbation. Typically this phase locking is achieved by passage through resonance with some initial equilibrium. In our case, we assume linearly chirped driving frequency $\Omega_d'(\tau) = 1 - \alpha\tau$ for simplicity, proceed from $\theta \approx 0$ ($m_z = 1$) at large negative time, and slowly pass the resonance $\Omega_d' = 1$ at $\tau = 0$. For small θ Eqs. (5) and (6) can be written as

$$\frac{d\theta}{d\tau} = -\varepsilon\sin\Phi, \tag{7}$$

$$\theta\frac{d\Phi}{d\tau} = (\alpha\tau - \theta^2/2)\theta - \varepsilon\cos\Phi, \tag{8}$$

which can be transformed into a single complex equation for $\Psi = \theta e^{i\Phi}$

$$i\frac{d\Psi}{d\tau} + (\alpha\tau - |\Psi|^2/2)\Psi = \varepsilon. \tag{9}$$

This NLS-type equation was studied in many applications and yields efficient phase locking at $\Phi \approx \pi$ after passage through linear resonance at $\tau = 0$, provided ε exceeds a threshold [37]

$$\varepsilon_{\text{th}} = 0.58\alpha^{3/4}. \tag{10}$$

Later (for $\tau > 0$), the phase locking continues as the nonlinear frequency shift follows that of the driving frequency, i.e., $\theta^2/2 \approx \alpha\tau$. Importantly, this continuing phase locking is characteristic of any variation of the driving frequency [then α in (9) represents the local frequency chirp rate at the

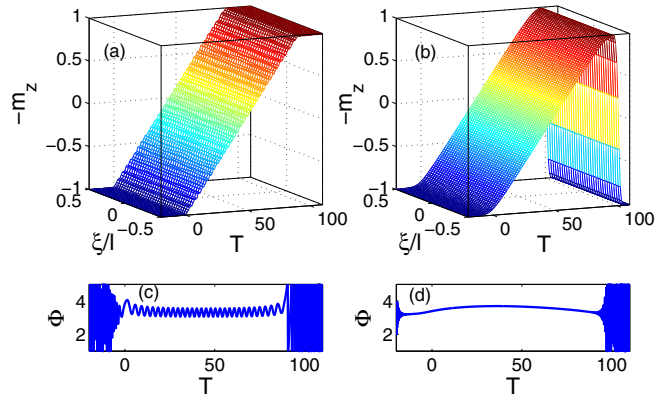

FIG. 1. The uniform autoresonant magnetization state. (a) z component of magnetization $-m_z$ versus slow time $T = \alpha^{1/2}\tau$; (c) phase mismatch $\Phi(0, T) = \phi - \phi_d$. In both panels $\lambda = 0$ and $\varepsilon = 3 \times 10^{-3}$. Panels (b) and (d) are the same as (a) and (c), but $\lambda = 3 \times 10^{-3}$ and $\varepsilon = 3 \times 10^{-2}$.

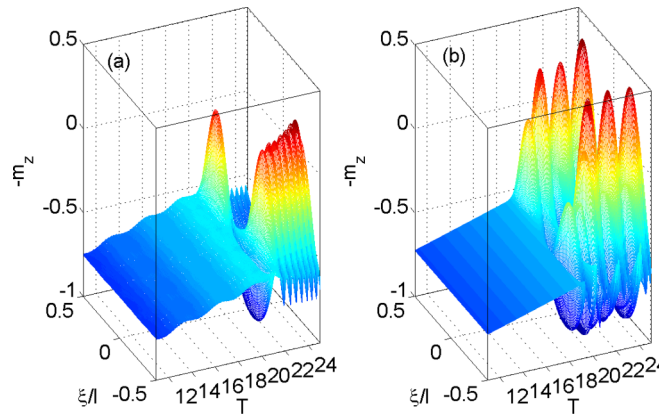

FIG. 2. The instability of the uniform magnetization state. The parameters of the simulations in (a) and (b) are the same as in Figs. 1(a) and 1(b), respectively, but $\kappa = 2\pi/l < 1$. A complex spatiotemporal magnetization profile develops beyond the point of instability.

initial resonance], while the system remains in an approximate nonlinear resonance

$$m_z = \cos\theta \approx \Omega_d'(\tau), \tag{11}$$

as long as the driving frequency chirp rate remains sufficiently small. Under these conditions, the magnetization angles θ and $\varphi \approx \varphi_d + \pi$ are efficiently controlled by simply varying the driving frequency. We illustrate this effect in Fig. 1, showing the results of numerical simulations of the original system (1), assuming spatial periodicity of length $l = 6$ and linearly chirped frequency $\Omega_d'(\tau) = 1 - \alpha\tau$. The initial conditions $\theta = 0.01|\cos(\kappa\xi)|$ ($\kappa = 2\pi/l$) represented a small spatial perturbation for studying stability of the uniform state and we used parameters $\lambda = 0$, $h_0 = 5$, $\varepsilon = 3 \times 10^{-3}$, and $\alpha = 5 \times 10^{-4}$ in Figs. 1(a) and 1(c), while $\lambda = 3 \times 10^{-3}$ and $\varepsilon = 3 \times 10^{-2}$ in Figs. 1(b) and 1(d). Our numerical scheme used an equivalent system of two coupled NLS-type equations based on the quantum two-level analog [29,38] described in the Appendix. Figures 1(a) and 1(b) (without and with damping, respectively) show the evolution of $-m_z = -\cos\theta$ versus slow time $T = \alpha^{1/2}\tau$, which approximately follows the linear time dependence $\cos\theta \approx \Omega_d'$ on time, while Figs. 1(c) and 1(d) represent the corresponding phase mismatch $\Phi(0, T) = \varphi(0, T) - \varphi_d(T)$ and illustrate the continuing azimuthal phase locking in the system at $\Phi \approx \pi$. Note that the uniform solution in this case is stable with respect to spatial perturbations. The dissipation changes the threshold condition for entering the autoresonant uniform state [29,39], has some effect on the phase mismatch [compare Figs. 1(c) and 1(d)], and leads to the collapse of the solution to the initial equilibrium after dephasing. Nevertheless, in the phase-locked stage the autoresonant uniform solutions are similar with and without damping and remains stable with respect to spatial perturbations. Note that a similar evolution can be obtained by starting from the $m_z = -1$ equilibrium if one applies the external magnetic field in the $-\hat{\mathbf{e}}_z$ direction ($h_0 < 0$). The driving field in this case must rotate in the opposite direction and the linear resonance takes place at the driving frequency $\Omega_d(\tau) = 1 + |h_0|$. With this modification, Fig. 1 and other figures below illustrating $m_z(\xi, T)$ remain the same if one changes the label $-m_z$ to m_z.

In contrast to the example in Fig. 1, one observes a spatial instability of the autoresonant uniform state in Figs. 2(a) and 2(b), showing the numerical simulations with the same parameters as in Figs. 1(a) and 1(b), but $l = 8$ instead of 6. One can see the destruction of the uniform state in Fig. 2 and formation of a complex spatiotemporal structure of $m_z(\xi, T)$ starting $T \approx 21$ in Fig. 1(a) and somewhat earlier in Fig. 1(b). These results can be explained by a perturbation theory as described below. We neglect damping for simplicity, freeze the time at $\tau = \tau_0$, and set $\Phi = \pi + \delta\Phi$ and $\theta = \theta_0 + \delta\theta$, where θ_0 satisfies

$$\cos\theta_0 - \Omega_d'(\tau_0) + \varepsilon\cot\theta_0 = 0. \tag{12}$$

Then, for small perturbations $\delta\Phi$ and $\delta\theta$ of frequency ν and wave vector κ, Eqs. (3) and (4) become

$$\begin{aligned} -i\nu\delta\theta &= -(\kappa^2\sin\theta_0 - \varepsilon)\delta\Phi, \\ -i\nu\delta\Phi &= \left(-\sin\theta_0 + \frac{\kappa^2}{\sin\theta_0} - \frac{\varepsilon}{\sin^2\theta_0}\right)\delta\theta, \end{aligned} \tag{13}$$

yielding

$$\nu^2 = \frac{1}{\sin^2\theta_0}(\kappa^2\sin\theta_0 - \varepsilon)(-\sin^3\theta_0 + \kappa^2\sin\theta_0 - \varepsilon). \tag{14}$$

One can see that for small ε, the uniform solution is stable with respect to spatial perturbations provided

$$\kappa > \sin\theta_0. \tag{15}$$

The examples in Figs. 1 ($\kappa = 1.047$) and 2 ($\kappa = 0.785$) are consistent with this result.

III. TRANSFORMATION FROM SPATIALLY UNIFORM SOLUTION TO A STANDING WAVE

The formation of a uniform autoresonant solution $\cos\theta_0(\tau) \approx \Omega_d'(\tau)$ in the spatially periodic LLG problem was demonstrated above using a constant amplitude chirped

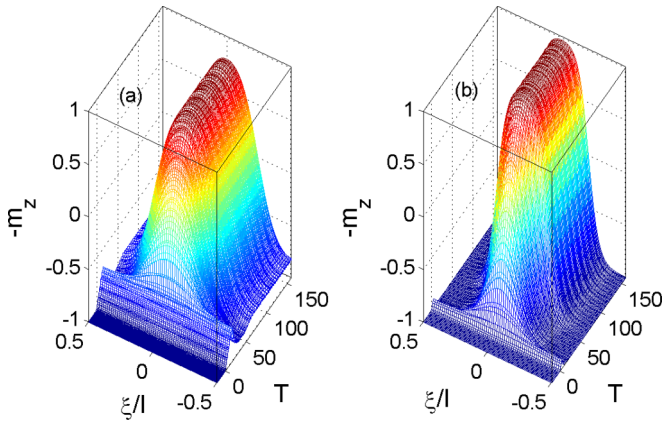

FIG. 3. The formation of autoresonant standing waves from the uniform magnetization state: (a) $\kappa = 0.78$, (b) $\kappa = 0.45$. The final waveform is reached as the driving frequency gradually decreases and stays constant for $T > 69$.

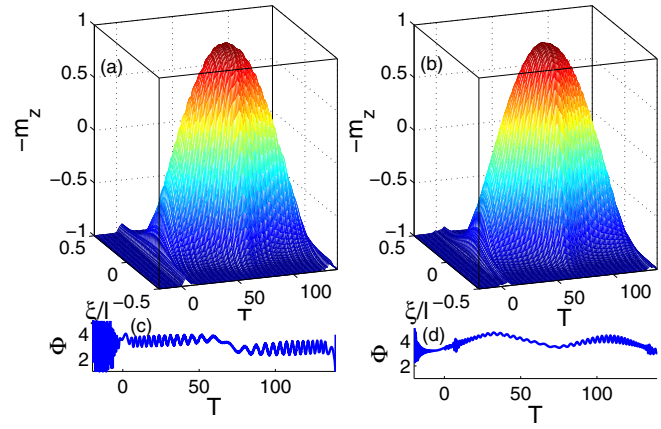

FIG. 4. The control of the phase-locked standing magnetization wave by varying the driving frequency. In (a) and (c) the parameters of the simulations are the same as in Fig. 3(b), but after reaching its minimal value at $T = 69$, the driving frequency increases back to the initial value, while the magnetization returns to the initial state. Panels (b) and (d) show $-m_z$ and phase mismatch Φ, respectively, versus slow time in the same case as (a) and (c), but $\lambda = 10^{-3}$ and $\varepsilon = 10^{-2}$.

frequency drive, yielding stable evolution provided the inequality (15) is satisfied (see Fig. 1). If during the evolution, this inequality is violated, the spatial instability develops (see Fig. 2). However, one can avoid the instability and transform the uniform autoresonant solution into an autoresonant standing wave by adding a simple spatial modulation of the driving amplitude, i.e., uses $\varepsilon = \varepsilon_0 + \varepsilon_1 \cos(\kappa\xi)$. We illustrate this phenomenon via simulations in Fig. 3, where we use parameters $\alpha = 5 \times 10^{-4}$ and $\lambda = 0$, but, in the driving term, apply a modulated drive with $\varepsilon_1 = \varepsilon_0 = 3 \times 10^{-3}$ and switch on ε_1 at $\tau = 0$. The chirped driving frequency in this numerical example is of form $\Omega_d' = 1 - \Delta\Omega \sin(\alpha\tau/\Delta\Omega)$ for $\tau < \pi\Delta\Omega/2\alpha$ and $\Omega_d' = 1 - \Delta\Omega$ for $\tau > \pi\Delta\Omega/2\alpha$, and we use $\Delta\Omega = 0.98$. Thus, as in previous illustrations, the frequency passes the resonance at $\tau = 0$ having chirp rate α but then gradually decreases reaching a constant. Figure 3(a) (where we use $l = 8$) shows that the addition of the spatial modulation of the driving amplitudes prevents the spatial instability and leads to the emergence of a growing amplitude standing wave solution. Figure 3(b) (where $l = 13$) shows a similar dynamics, yielding formation of larger amplitude standing wave, which starts earlier, at $T \approx 5$ (we again use the slow time $T = \alpha^{1/2}\tau$ in this and the following figures). The excited standing wave is fully controlled by the variation of the driving frequency and precesses azimuthally with the angular velocity of the driving phase (due to the continuing phase locking of $\Phi \approx \pi$). Furthermore, the magnetization waveform is spatially locked to the driving perturbation, while the wave amplitude and form is controlled by the instantaneous frequency of the drive. Importantly, as l increases, the maximum and the minimum of the final solution for m_z become near $+1$ and -1, respectively. We have also verified numerically that this solution approaches the well known soliton form with exponentially falling tails [see Eq. (6.21) in Ref. [9]]. We further illustrate the autoresonant control of the standing magnetization waves in Figs. 4(a) and 4(c), where we show the results of simulations with all the parameters of Fig. 3(b), but instead of saturating the driving frequency, we allow it to vary according to the same sinusoidal formula for an additional time interval $\pi\Delta\Omega/2\alpha < \tau < \pi\Delta\Omega/2\alpha$, so the frequency returns to its original value. Figures 4(b) and 4(d) show the results of similar simulations with the same parameters as in Figs. 4(a) and 4(c), but $\varepsilon = 10^{-2}$ and $\lambda = 10^{-3}$. One observes the return of the magnetization to its initial uniform state, being continuously phase locked [see Figs. 4(c) and 4(d)] to the drive with or without dissipation. The idea of the transformation from the uniform to standing wave solution by passage through the spatial instability originates from the similarity to the autoresonant excitations of standing waves of the driven-chirped nonlinear Schrodinger (NLS) equation [31]:

$$i\psi_\tau + \psi_{\xi\xi} + |\psi|^2\psi + \varepsilon e^{-i\int \omega_d d\tau} = 0. \tag{16}$$

If one writes $\psi = ae^{-i\phi}$ and separates the real and imaginary parts in (16), one arrives at the system

$$a_\tau = a\Phi_{\xi\xi} + 2\Phi_\xi a_\xi - \varepsilon \sin\Phi, \tag{17}$$

$$\Phi_\tau = -\frac{a_{\xi\xi}}{a} + \Phi_\xi^2 - a^2 - \omega_d(t) - \frac{\varepsilon}{a}\cos\Phi, \tag{18}$$

where $\Phi = \phi - \int \omega_d d\tau$. Similarly to our ferromagnetic problem, the passage through the linear resonance in this system yields excitation of the uniform autoresonant NLS solution followed by transformation into autoresonant standing wave [31]. One notices the structural similarity between this NLS system and LLG Eqs. (3) and (4), so we proceed to the theory for the magnetization case using the driven NLS ideas.

We assume that the time evolution in Eqs. (3) and (4) is slow and interpret the solutions at a given time τ, as being a slightly perturbed solution of the same system of equations but with the time derivatives and the forcing terms set to zero, i.e.,

$$\Phi_{\xi\xi}\sin\theta + 2\Phi_\xi\theta_\xi\cos\theta = 0,$$
$$\left(-\frac{1}{\sin\theta}\theta_{\xi\xi} + \Phi_\xi^2\cos\theta\right) - \Omega_d'(\tau) + \cos\theta = 0. \tag{19}$$

We notice that this is a dynamical, two degrees of freedom problem (ξ serving as "time") governed by Hamiltonian

$$H = \tfrac{1}{2}\left(\theta_\xi^2 + \Phi_\xi^2 \sin^2\theta\right) + V(\theta), \tag{20}$$

where

$$V(\theta) = -\Omega_d'(\tau)\cos\theta + \tfrac{1}{4}\cos(2\theta). \tag{21}$$

This fixed τ problem is integrable since it conserves the canonical momentum $B = \Phi_\xi \sin^2\theta$ and energy

$$E = \tfrac{1}{2}\theta_\xi^2 + V_{\text{eff}}, \tag{22}$$

where $V_{\text{eff}}(\theta,\tau) = \frac{B^2}{2\sin^2\theta} + V(\theta)$. Next, we discuss oscillating solutions of this problem and introduce the conventional action-angle variables (I,Θ) and (B,Φ), where the first pair describes pure θ oscillations in the effective potential V_{eff}, while the second pair is associated with the dynamics of Φ. If one returns to the original (time dependent and driven) system (3) and (4), $E(\tau)$ and $B(\tau)$ become slow functions of time. We will present a theory describing these slow parameters via Whitham's average variational principle [36] in the next section and devote the remaining part of the current section to a simple qualitative picture of the dynamics. Our qualitative picture is based on the assumption of *almost* purely θ dynamics in the problem, i.e., setting $B \approx 0$, which means a continuous phase locking $\Phi \approx \pi$, simplifying the effective potential to $V_{\text{eff}} \approx -\Omega_d'(\tau)\cos\theta + \frac{1}{4}\cos(2\theta)$. As already discussed above, the phase locking at π is guaranteed in the initial excitation stage via temporal autoresonance with constant amplitude $\varepsilon = \varepsilon_0$, chirped frequency perturbation. But now our driving amplitude $\varepsilon = \varepsilon_0 + \varepsilon_1\cos(\kappa\xi)$ has two terms, where the first leads to excitation of the uniform autoresonant solution as discussed above, while the second term yields transition to the standing wave solution. Initially, θ is efficiently trapped at the minimum location θ_m of the potential well V_{eff} given by $\cos\theta_m = \Omega_d'(\tau)$. To $O(\varepsilon)$ this yields $\theta \approx \theta_m$, so this dynamics corresponds to the uniform autoresonant solution [see Eq. (12)]. The second term $\varepsilon_1\cos(\kappa\xi)$ in the driving has little effect on the evolution at this stage, until the spatial frequency $\kappa_0 = \sqrt{\partial^2 V_{\text{eff}}/\partial\theta_m^2}$ of oscillations of θ around θ_m passes the resonance with this driving term, i.e., when

$$\Omega_d'(\tau)\cos\theta_m - \cos(2\theta_m) \approx \sin^2\theta_m = \kappa^2. \tag{23}$$

But this is exactly the location of the instability of the uniform solution [see Eq. (15)] without the term $\varepsilon_1\cos(\kappa\xi)$ in the drive. The passage through the resonance with this new drive term excites growing amplitude oscillations of θ in the effective potential. After the passage, the oscillations of θ become autoresonant as the amplitude increases to preserve their spatial frequency near κ continuously. These newly induced spatially phase-locked, growing amplitude oscillations of θ comprise the autoresonant standing wave solution. The amplitude of these oscillations does not grow indefinitely. Indeed, when the potential V_{eff} becomes shallower again as θ_m passes $\pi/2$ at $\Omega_d'(\tau) = 0$, the spatial resonance cannot be sustained, and the autoresonance is expected to interrupt. We illustrate this dynamics in Fig. 5, showing the effective potential V_{eff} (thin red lines) at 14 successive values of slow time starting $T = -20$. The thick blue lines in the figure show the value of the potential at $\theta(\xi, T)$ at these times, as obtained in the simulations in the example in Fig. 3(a).

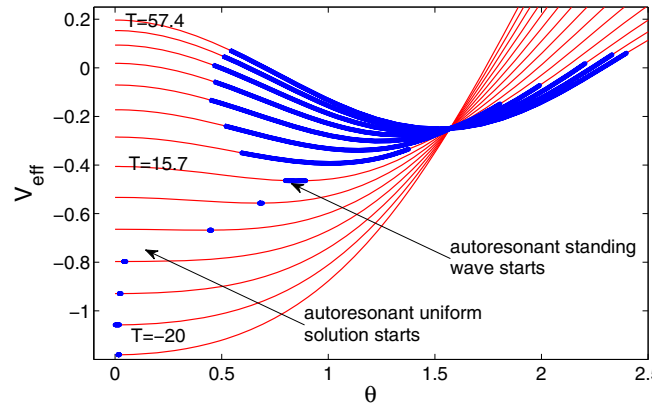

FIG. 5. The formation of the autoresonant standing wave modelled via dynamics of a quasiparticle in a slowly varying effective potential V_{eff}. V_{eff} versus θ is shown for successive times (thin red lines) starting at $T = -20$. The thick blue lines show spatial oscillations of θ at these times, as obtained in simulations in Fig. 3(a). The excitation proceeds as the quasiparticle remains at the bottom of the potential well continuously, corresponding to the flat solution. After passage through resonance with the spatial modulation of the driving amplitude, autoresonant oscillations of the quasiparticle in the effective potential are excited, describing the standing magnetization wave.

IV. WHITHAM'S AVERAGED VARIATIONAL ANALYSIS

A. Averaged Lagrangian density

The LLG problem governed by Eqs. (3) and (4) allows Lagrangian formulation with the Lagrangian density $L = L_0 + L_1$ where

$$L_0(\theta,\theta_\xi,\Phi_\tau,\Phi_\xi,\tau) = \tfrac{1}{2}\left(\theta_\xi^2 + \Phi_\xi^2\sin^2\theta\right) + \Phi_\tau\cos\theta + \Omega_d'(\tau)\cos\theta - \tfrac{1}{4}\cos(2\theta) \tag{24}$$

and the perturbing part

$$L_1 = -\varepsilon\sin\theta\cos\Phi. \tag{25}$$

For studying the slow autoresonant evolution in system (3) and (4), we use Whitham's averaged Lagrangian approach. Following Refs. [31,40], describing a similar NLS problem, we seek solutions of form

$$\theta = \vartheta(\tau) + U(\Theta,\tau),\ \Phi = \upsilon(\tau) + V(\Theta,\tau), \tag{26}$$

where the explicit time dependence is slow, while $\Theta(\xi,\tau)$ is a fast variable and U and V are 2π periodic in Θ. In addition, the frequencies $\Theta_\tau = -\Omega(\tau)$ and $\beta = \upsilon_\tau$ are slow functions of time and the wave vector $\Theta_\xi = \kappa = const$ ($\kappa = 2\pi/l$, l being the periodicity length in our problem). The Whitham's averaging [36] in this system proceeds from the unperturbed Lagrangian density L_0, where one *freezes* the slow time dependence at some τ and, using $\Phi_\xi = \kappa V_\Theta$, replaces $\Phi_\tau = \beta - \Omega V_\Theta = \beta - (\Omega/\kappa)\Phi_\xi$. This yields

$$L_0 = \frac{1}{2}\left(U_\xi^2 + \Phi_\xi^2\sin^2\theta\right) + \left(\beta + \Omega_d' - \frac{\Omega}{\kappa}\Phi_\xi\right)\cos\theta - \frac{1}{4}\cos(2\theta). \tag{27}$$

Recall that the explicit dependence on U in (27) enters via $\theta = \vartheta + U$. This Lagrangian density describes a two degrees of freedom dynamical problem (for U and Φ), where ξ plays the role of "time." In dealing with this problem we use Hamiltonian formulation. We define the usual canonical momenta

$$P^U = \partial L_0/\partial U_\xi = U_\xi \tag{28}$$

$$P^\Phi = \partial L_0/\partial \Phi_\xi = \Phi_\xi \sin^2\theta - \frac{\Omega}{\kappa}\cos\theta \tag{29}$$

and observe that Φ is a cyclic variable and therefore $P^\Phi = B$ is the integral of motion. We will unfreeze the slow time dependence later and $B(\tau)$ will becomes a slow function of time. The Lagrangian density L_0 yields the Hamiltonian in the time-frozen problem

$$H_0 = P^U U_\xi + P^\Phi \Phi_\xi - L_0 \tag{30}$$

and, after some algebra,

$$H_0 = H_0'(P^\theta, \theta) + V_1(\theta, B, \Omega, \beta), \tag{31}$$

where

$$H_0'(P^U, U) = \tfrac{1}{2}(P^U)^2 + V(\theta) - V(\vartheta), \tag{32}$$

$$V(\theta) = -\Omega_d' \cos\theta + \tfrac{1}{4}\cos(2\theta), \tag{33}$$

and

$$V_1(B, \Omega, \beta, \theta) = V(\vartheta) + \frac{\left(B + \frac{\Omega}{\kappa}\cos\theta\right)^2}{2\sin^2\theta} - \beta\cos\theta.$$

At this stage, we return to the full driven (still time-frozen) problem governed by the Hamiltonian

$$H = H_0'(P^U, U) + V_1 - L_1 \tag{34}$$

(recall that $L_1 = -[\varepsilon_0 + \varepsilon_1\cos(\kappa\xi)]\sin\theta\cos\Phi$) and make canonical transformation from P^U, U to the action-angle (AA) variables I, Θ of Hamiltonian H_0'. The dynamics governed by this Hamiltonian conserves its energy $E = H_0'$ and is periodic of period 2π in Θ, and, at this stage, we identify Θ with the angle variable used in the definitions (26). The action variable in H_0' problem is

$$I = \frac{1}{2\pi}\oint P^U dU = \frac{1}{2\pi}\oint \sqrt{2[E - V(\theta) + V(\vartheta)]}dU, \tag{35}$$

where the time dependence enters both explicitly in V and via ϑ. Note that

$$\frac{\partial I}{\partial E} = \frac{1}{2\pi}\oint \frac{1}{\sqrt{2[E - V(\theta) + V(\vartheta)]}}dU = \frac{1}{\widetilde{\kappa}}, \tag{36}$$

$\widetilde{\kappa}(\vartheta, E)$ being the (spatial) frequency of the oscillations of U governed by H_0'. Next, we write the full Lagrangian in our problem in terms of the new action angle variables

$$L = \frac{d\Theta}{d\xi}I - H = \kappa I - E - V_1(B, \Omega, \beta, \theta) + L_1(\theta, \xi, \tau), \tag{37}$$

where $\theta = \vartheta + U(I, \Theta, \tau)$ in V_1 and L_1, as the result of the canonical transformation. The Whitham's averaged Lagrangian density Λ is obtained by averaging L in the time-frozen problem over one oscillation governed by H_0':

$$\Lambda = \frac{1}{2\pi}\int_0^{2\pi} L d\Theta = \kappa I - E - \frac{1}{2\pi}\int_0^{2\pi}(V_1 - L_1)d\Theta. \tag{38}$$

To complete the averaging, we calculate two remaining components $\langle V_1\rangle = \frac{1}{2\pi}\int_0^{2\pi} V_1 d\Theta$ and $\Lambda_1 = \frac{1}{2\pi}\int_0^{2\pi} L_1 d\Theta$ in (38).

$$\langle V_1\rangle = V(\vartheta) + \frac{1}{2\pi}\int_0^{2\pi}\left[\frac{\left(B + \frac{\Omega}{\kappa}\cos\theta\right)^2}{2\sin^2\theta} - \beta\cos\theta\right]d\Theta$$

$$= V(\vartheta) + I_1\frac{B^2}{2} + I_2\frac{B\Omega}{\kappa} + I_3\frac{\Omega^2}{2\kappa^2} - \beta I_4, \tag{39}$$

where $I_1 = \langle\frac{1}{\sin^2\theta}\rangle$, $I_2 = \langle\frac{\cos\theta}{\sin^2\theta}\rangle$, $I_3 = \langle\frac{\cos^2\theta}{\sin^2\theta}\rangle$, $I_4 = \langle\cos\theta\rangle$, and the averages $\langle\ldots\rangle$ are defined as

$$\langle\ldots\rangle = \frac{1}{2\pi}\int_0^{2\pi}(\ldots)d\Theta = \frac{\kappa}{2\pi}\oint\frac{(\ldots)}{\sqrt{2[E - V(\theta) + V(\vartheta)]}}dU. \tag{40}$$

Finally, we calculate the averaged driving part of the Lagrangian density (recall that $\theta = \vartheta + U$ and $\Phi = \upsilon + V$)

$$\Lambda_1 = -\frac{1}{2\pi}\int_0^{2\pi}[\varepsilon_0 + \varepsilon_1\cos(\kappa\xi)] \times \sin(\vartheta + U)\cos(\upsilon + V)d\Theta. \tag{41}$$

Here, we limit evaluation of this averaged object to small spatial oscillations of θ around ϑ, write $U \approx a(I)\cos\Theta$ and replace $\sin(\vartheta + U) \approx \sin\vartheta + a(I)\cos\vartheta\cos\Theta$. Furthermore, we will also assume that V is sufficiently small to replace $\cos(\upsilon + V) \approx \cos\upsilon$. Finally, assuming a continuous approximate double resonance in the problem, i.e., $\upsilon(\tau) - \pi = \upsilon' \approx 0$ and $\Theta - \kappa\xi - \pi = \mu(\tau) \approx 0$ (initial phase locking of υ at π was shown in the uniform autoresonant solution stage), after averaging

$$\Lambda_1 \approx \left(\varepsilon_0\sin\vartheta - \frac{\varepsilon_1}{2}a(I)\cos\vartheta\cos\mu\right)\cos\upsilon'. \tag{42}$$

Therefore, our final averaged Lagrangian becomes

$$\Lambda = \kappa I - E - V(\vartheta) - \frac{I_1 B^2}{2} - \frac{I_2 B\Omega}{\kappa} - \frac{I_3\Omega^2}{2\kappa^2} + I_4\beta + \left[\varepsilon_0\sin\vartheta - \frac{\varepsilon_1}{2}a(I)\cos\vartheta\cos\mu\right]\cos\upsilon'. \tag{43}$$

We discuss the slow evolution of the full driven system next. Following Whitham, this evolution is obtained by unfreezing the time and taking variations of Λ with respect to all dependent variables E, ϑ, B, Θ, and υ. Obviously, only slow objects enter the averaged Lagrangian density.

B. Evolution equations and stability analysis

At this stage, we write variational evolution equations. The variation of Λ with respect to B yields

$$\frac{d\mu}{d\tau} = -\Omega = \frac{\kappa I_1}{I_2}B, \tag{44}$$

and the variation with respect to Θ and use of (44) results in

$$\frac{d}{d\tau}\left[\left(I_2^2 - I_1 I_3\right)\frac{B}{\kappa I_2}\right] \approx \frac{\varepsilon_1}{2} a \cos\vartheta \sin\mu. \tag{45}$$

Similarly, the variation with respect to E and υ gives

$$I_{4E}\frac{d\upsilon'}{d\tau} = 1 - \frac{\kappa}{\widetilde{\kappa}} + B^2\left(\frac{I_{1E}}{2} - \frac{I_{2E} I_1}{I_2} + \frac{I_{3E} I_1^2}{2 I_2^2}\right) + \frac{\varepsilon_1}{2} a_E \cos\vartheta \cos\mu \cos\upsilon' \tag{46}$$

and

$$\frac{dI_4}{d\tau} \approx -\left(\varepsilon_0 \sin\vartheta - \frac{\varepsilon_1}{2} a \cos\vartheta \cos\mu\right)\sin\upsilon'. \tag{47}$$

Finally, the variation with respect to ϑ yields

$$I_{4\vartheta}\frac{d\upsilon'}{d\tau} = \frac{\partial V(\vartheta)}{\partial\vartheta} - \kappa\frac{\partial I}{\partial\vartheta} + B^2\left(\frac{I_{1\vartheta}}{2} - \frac{I_{2\vartheta} I_1}{I_2} + \frac{I_{3\vartheta} I_1^2}{2 I_2^2}\right) - \left(\varepsilon_0 \cos\vartheta + \frac{\varepsilon_1}{2} a \sin\vartheta \cos\mu\right)\cos\upsilon'. \tag{48}$$

Equations (44)–(48) comprise a complete set of slow evolution equations for E, B, μ, υ', and ϑ. The solution of these equations proceeds by defining a quasisteady state $B_0 = \mu_0 = \upsilon_0' = 0$, $\vartheta = \vartheta_0$ and E_0 given by

$$(V_\vartheta - \kappa I_\vartheta)_{E_0,\vartheta_0} - \varepsilon_0 \cos\vartheta_0 - \frac{\varepsilon_1}{2} a \sin\vartheta_0 = 0, \tag{49}$$

$$G(E_0, \vartheta_0) = \left(1 - \frac{\kappa}{\widetilde{\kappa}} + \frac{\varepsilon_1}{2} a_E \cos\vartheta_0\right)_{E_0,\vartheta_0} = 0. \tag{50}$$

Note that in the case $\varepsilon_1 = 0$ and small E, Eq. (49) nearly coincides with Eq. (12) describing the autoresonant uniform solution. Furthermore, for small E, to $O(\varepsilon)$, Eq. (49) yields $V_{\vartheta_0} \approx 0$, i.e., ϑ_0 remains near the location of the minimum of $V(\theta)$ given by $\cos\vartheta_0 \approx \Omega_d'$, as was suggested in the qualitative model in Sec. IV and seen in simulations. On the other hand, Eq. (50) clarifies the phase locking at $\mu \approx 0$ as $\widetilde{\kappa}$ approaches the resonance $\widetilde{\kappa} = \kappa$ from below.

Despite the formal complexity of the averaged variational theory, it now allows us to easily find the quasisteady state of the magnetization versus time in this chirped-driven problem without solving the LLG equation numerically. We illustrate such a calculation in Fig. 6. The dots in panel (a) in the figure represent the quasienergy E versus time found by solving algebraic equation (50) in the two examples in Fig. 3. The solid lines in the same panel show the energy $\frac{1}{l}\int_0^l H_0'(\xi)d\xi$ from our numerical simulations, where H_0' is defined in Eq. (32). Panel (b) in the figure shows by dots the magnetization waveform $m_z(\xi) = \cos\vartheta$ found by quadratures, i.e., by solving $\frac{1}{2}(d\vartheta/d\xi)^2 + V(\vartheta) = E$. The solid lines in this panel show the results from the numerical simulations. One can see that the agreement between the quasisteady state theory and simulations is excellent. In contrast to the simplicity of finding the quasisteady state via the variational theory, the analysis

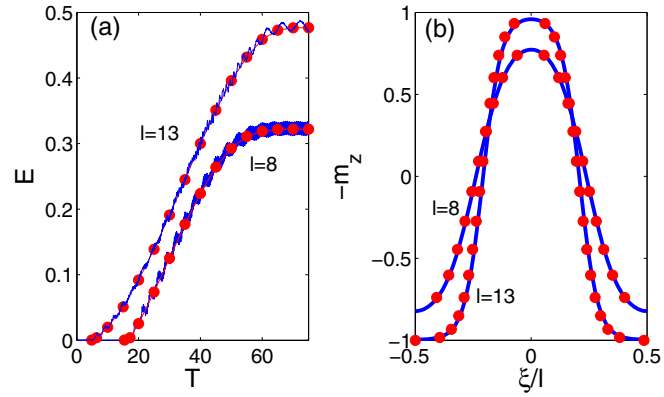

FIG. 6. Comparison between the quasisteady state solution from the variational theory (dots) and numerical simulations (solid lines). Panel (a) presents the quasienergy E versus time in the two examples in Fig. 3, while panel (b) shows the waveform $m_z(z)$ in the same examples at time $T = 70$.

of its stability illustrated in numerical simulations is more complex and is discussed below.

For small perturbations $\delta E, \delta B, \delta\mu, \delta\upsilon'$, and $\delta\vartheta$ of the quasisteady state, we use $I \approx \delta E/\widetilde{\kappa} \approx \delta E/\sin\vartheta_0$ to get the lowest order (linear) set of equations

$$\frac{d\delta\mu}{d\tau} = \frac{\kappa I_1}{I_2}\delta B, \tag{51}$$

$$\frac{d\delta B}{d\tau} = -\frac{\kappa\varepsilon_1 a I_2 \cos\vartheta_0}{2\left(I_1 I_3 - I_2^2\right)}\delta\mu, \tag{52}$$

$$I_{4E}\frac{d\delta\upsilon'}{d\tau} = G_\vartheta \delta\vartheta + G_A \delta E, \tag{53}$$

$$I_{4E}\frac{d\delta E}{d\tau} + I_{4\vartheta}\frac{d\delta\vartheta}{d\tau} = -\left(\varepsilon_0 \sin\vartheta_0 - \frac{\varepsilon_1}{2} a \cos\vartheta_0\right)\delta\upsilon', \tag{54}$$

$$I_{4\vartheta}\frac{d\delta\upsilon'}{d\tau} = V_{\vartheta\vartheta}\delta\vartheta - \kappa R \delta E, \tag{55}$$

where we use $\widetilde{\kappa} \approx \sin\vartheta_0$, so $R \approx \cos\vartheta_0/\sin^2\vartheta_0$ and all coefficients in (51)–(55) are viewed as constants evaluated at the quasisteady state. Equations (51) and (52) yield

$$\frac{d^2\delta\mu}{d\tau^2} + \nu_1^2\delta\mu \approx 0, \tag{56}$$

while Eqs. (53)–(55) reduce to

$$\frac{d^2\delta\upsilon'}{d\tau^2} + \nu_2^2\delta\upsilon' \approx 0, \tag{57}$$

where the two frequencies satisfy

$$\nu_1^2 = \frac{\varepsilon_1\kappa^2 I_1 a\cos\vartheta_0}{2\left(I_1 I_3 - I_2^2\right)},$$

$$\nu_2^2 = \frac{\left(\varepsilon_0\sin\vartheta_0 - \frac{\varepsilon_1}{2}a\cos\vartheta_0\right)\left(G_E V_{\vartheta\vartheta} - \kappa R G_\vartheta\right)}{I_{4E}\left(I_{4E}V_{\vartheta\vartheta} - \kappa R G_\vartheta\right) + I_{4\vartheta}\left(G_E I_{4\vartheta} - G_\vartheta I_{4E}\right)}.$$

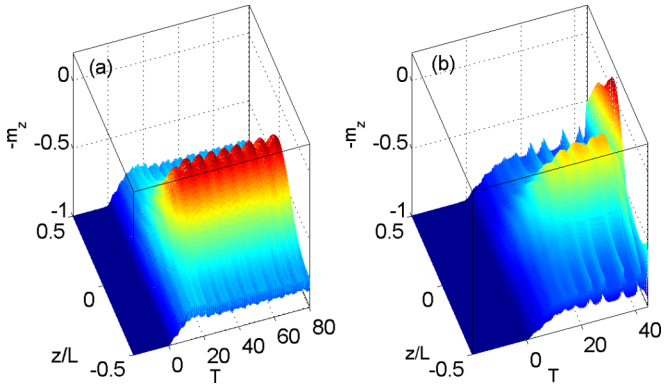

FIG. 7. The transition to instability of the autoresonant magnetization wave. The parameters are as those in Fig. 3(a), but a larger final driving frequency (smaller excitation amplitude) and different ε_1. Panels (a) and (b) show the excited waveforms for $\varepsilon_1/\varepsilon_0 = 9$ and 11, respectively, i.e., below and above the instability threshold $\varepsilon_1/\varepsilon_0 = 9.8$. The spatial phase locking is lost for $T > 40$ in panel (b).

A positiveness of $\nu_{1,2}^2$ guarantees stability of the (doubly) autoresonant ($\upsilon' \approx 0$ and $\mu \approx 0$) evolution of the system. We observe that

$$I_1 I_3 - I_2^2 \propto \left(\sum_i \frac{1}{s_i}\right)\left(\sum_j \frac{x_j^2}{s_j}\right) - \left(\sum_i \frac{x_i}{s_i}\right)^2,$$

where $x_i = \cos\theta_i$ and $s_i = \sin^2\theta_i\sqrt{[E - V_{\rm eff}(\theta_i)]}$. Then

$$I_1 I_3 - I_2^2 \propto \sum_{i,j>i} \frac{(x_i - x_j)^2}{s_i s_j}, \tag{58}$$

so ν_1^2 is positive for $\vartheta_0 < \pi/2$. Then, since $B = \delta B$, and $\mu = \delta\mu$, they both remain small. Furthermore, for small excitations of E, to lowest order in E, $\kappa = \sin\vartheta_0$, $G_\vartheta = \cos\vartheta_0/\sin\vartheta_0$, $G_E = (\frac{1}{\sin\vartheta_0} - \frac{3}{2\sin^3\vartheta_0})$, $I_{4\vartheta} = -\sin\vartheta_0$, $I_{4E} = \cos\vartheta_0/\sin^2\vartheta_0$. With these substitutions, one finds $\nu_2^2 \approx \varepsilon_0\sin\vartheta_0 - \frac{\varepsilon_1}{2}a\cos\vartheta_0$. Then condition $\varepsilon_0\sin\vartheta_0 - \frac{\varepsilon_1}{2}a\cos\vartheta_0 > 0$ guarantees the stability of the autoresonant evolution. We illustrate this conclusion in Fig. 7, showing the results of numerical simulations for parameters of Fig. 3(a), but $\Delta\Omega = 0.4$, i.e., larger final driving frequency $\Omega' = 1 - \Delta\Omega$ and, thus, smaller excitation amplitude a. We estimate numerically that in this case $\vartheta_0 \approx 0.89rad$ and $a \approx 0.25rad$. This yields the transition to instability at $\varepsilon_1/\varepsilon_0 = 2\sin\vartheta_0/(a\cos\vartheta_0) \approx 9.8$. Panels (a) and (b) in Fig. 7 show the excited magnetization waveform for $\varepsilon_1/\varepsilon_0 = 9$ and 11, respectively. One can see that below the instability condition ($\varepsilon_1/\varepsilon_0 = 9$) the excited wave remains spatially phase locked to the drive, arriving at the final quasisteady state at later times. In contrast, for $\varepsilon_1/\varepsilon_0 = 11$ in panel (b), the initial excitation stage is similar to that in panel (a), but the spatial phase locking is lost beyond $T \approx 40$ due to the instability and the magnetization develops a complex spatiotemporal profile.

V. ALTERNATIVE DRIVING SCHEMES

Here we discuss two modifications of the driving component in the LLG equation (1), which may allow the required submicron spatial modulation of the drive. The first modification is using spin torque drive instead of the microwave (a related autoresonant problem for single domain nanoparticles was studied in Ref. [30]). The effective magnetic field associated with the spin torque is

$$\mathbf{h}_s = \mathbf{m} \times \mathbf{I}_s, \tag{59}$$

where $\mathbf{I}_s$ is the dimensionless spin polarized current, which will be assumed of form $\mathbf{I}_s = 2\varepsilon\sin\varphi_d\mathbf{e}_x$ in the following, yielding $\mathbf{h}_s = 2\varepsilon(m_z\mathbf{e}_y - m_y\mathbf{e}_z)$, and possibly using nanocontacts [41] for submicron spatial modulation of ε. The analog of system (3), (4) for this drive is

$$\theta_\tau = \Phi_{\xi\xi}\sin\theta + 2\Phi_\xi\theta_\xi\cos\theta - \varepsilon\cos\theta\sin\Phi, \tag{60}$$

$$\Phi_\tau = \left(-\frac{1}{\sin\theta}\theta_{\xi\xi} + \Phi_\xi^2\cos\theta\right) - \Omega_D' - \frac{\varepsilon\cos\Phi}{\sin\theta}, \tag{61}$$

where $\Phi = \varphi - \varphi_d + \pi/2$. Note that for small θ the last two equations are nearly the same as Eqs. (3), (4) for the microwave drive. One consequence of this is that the autoresonance threshold when passing the linear resonance is the same for both cases. Figure 8(a) illustrates the formation and control of the autoresonant standing wave via a spin torque drive in simulations using the parameters of Fig. 3(b). One can see that the form of the excited solution in Figs. 3(b) and 8(a) are very similar. Despite this similarity, a complete Whitham's-type theory of the spin torque driven problem is more complex than that for the microwave drive case, because the driving parts in Eqs. (60) and (61) do not allow Lagrangian description. Therefore, we leave this theory outside the scope of the present work.

The second driving alternative is using the same chirped frequency microwave drive of uniform amplitude ε_0, but

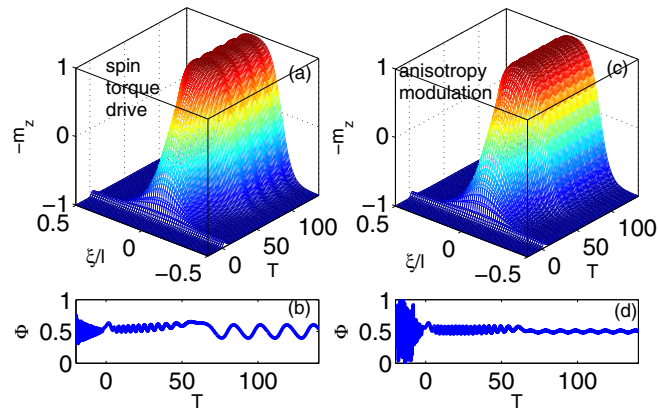

FIG. 8. Formation of the autoresonant standing magnetization wave by chirped frequency spin torque drive [panel (a)] and via a combination of a uniform AC drive and a modulation of the hard axis anisotropy [panel (c)]. The parameters in the simulations are the same as in Fig. 3(b) for the AC drive, while for the anisotropy modulation case $\varepsilon_2 = -2.5\varepsilon_0$. Panels (b) and (d) show the corresponding phase mismatch $\Phi(0, T)$ for the two drives, respectively.

adding a spatially modulated [42] hard axis anisotropy in the system (along $\widehat{\mathbf{e}}_x$, for example). The driving component of the effective field in this case will become

$$\mathbf{h}_d = \varepsilon_0(\cos\varphi_d\widehat{\mathbf{e}}_x + \sin\varphi_d\widehat{\mathbf{e}}_y) - 2\varepsilon_2\cos(\kappa\xi)m_x\widehat{\mathbf{e}}_x, \quad (62)$$

$2\varepsilon_2$ being the ratio between the easy and hard axis anisotropy coefficients. In the autoresonance, $m_x = \sin\theta\cos\varphi \approx -\sin\theta\cos\varphi_d$ and one can rewrite $\mathbf{h}_d$ as

$$\mathbf{h}_d \approx [\varepsilon_0 + \varepsilon_2\sin\theta\cos(\kappa\xi)](\cos\varphi_d\widehat{\mathbf{e}}_x + \sin\varphi_d\widehat{\mathbf{e}}_y) \quad (63)$$
$$+ \varepsilon_2\sin\theta\cos(\kappa\xi)(\cos\varphi_d\widehat{\mathbf{e}}_x - \sin\varphi_d\widehat{\mathbf{e}}_y).$$

The last term in this expression is rotating in the opposite direction and, being nonresonant, has a negligible effect. Thus, effectively, $\mathbf{h}_d$ has a form similar to that analyzed in our theory for the microwave drive. Figure 8(b) illustrates this idea in simulations using $\mathbf{h}_d$ from Eq. (62) and the same parameters as in Fig. 8(a), but $\varepsilon_1 = 0$ and $\varepsilon_2 = 1.25\varepsilon_0$. We see that this different combination drive yields a very similar autoresonant magnetization wave as in Figs. 3(b) and 8(a). Furthermore, we have seen numerically that within this driving scheme, one can excite large amplitude autoresonant waves with the modulation scale reaching $L = 1000$ nm using smaller driving amplitudes and chirp rates. However, this may limit some experiments, because it also requires a weaker dissipation for stable evolution.

VI. CONCLUSIONS

In conclusion, we have studied the problem of autoresonant excitation and control of 1D standing magnetization waves in an easy axis ferromagnetic in an external magnetic field and driven by a weak circularly polarized, chirped frequency microwave field. We had modeled this problem by the spatially periodic time dependent LLG equation [see Eq. (1)]. We had discussed the excitation of the autoresonant solutions in this system via theory and compared the results with numerical simulations. The excitation proceeded as the driving frequency passed a resonance with the initially spatially uniform magnetization equilibrium in the direction of the easy axis (polar angle $\theta = 0$), yielding a driven spatially uniform magnetization with the azimuthal angle φ of the magnetization locked (and therefore controlled) by the phase of the microwave. This phase locking (autoresonance) reflects a continuous self-adjustment of θ [see Eq. (11)], so that the resonance is preserved despite the variation of the driving frequency. It was shown that the condition for this autoresonant evolution is the driving amplitude ε exceeding a threshold, which scales with the driving frequency chirp rate as $\varepsilon_{\text{th}} \sim \alpha^{3/4}$ [see Eq. (10)]. We had also shown that the uniform autoresonant magnetization state remained stable with respect to spatial perturbations if $\sin\theta < \kappa = 2\pi/l$, l being the periodicity length in the problem. In the case $2\pi/l > 1$, the stable uniform state reached a complete magnetization inversion ($\theta \to \pi$). In contrast, when θ increased during the autoresonant uniform state evolution and passed the point where $\sin\theta = 2\pi/l$, the spatial instability developed, yielding a complex spatiotemporal magnetization wave form.

We had shown that if instead of a constant driving amplitude, one introduced a spatially modulated amplitude $\varepsilon_0 + \varepsilon_1\cos(\kappa\xi)$, then, instead of the instability, a standing wave is excited with the amplitude and form controlled by the frequency of the driving wave. This emerging autoresonant solution is doubly phase locked, i.e., its azimuthal angle φ is locked to the phase of the driving wave, while θ performs slowly evolving growing amplitude nonlinear spatial oscillations in an effective potential, which are continuously phase locked to the spatial modulation of the drive. Furthermore, as the periodicity length l increases, the autoresonant wave approaches the well know soliton form [see Eq. (6.21) in Ref. [9]]. The formation of the autoresonant standing wave is fully reversible and can be returned to its initial uniform ($\theta \approx 0$) state by simply reversing the variation of the driving frequency. In addition to suggesting a qualitative description of this autoresonant evolution (see Sec. III), we had developed a complete theory of the dynamics in the problem based on the Whitham's averaged variational approach and studied modulational stability of the autoresonant solutions (see Sec. IV). We had found numerically that a sufficiently weak dissipation does not affect the autoresonant evolution significantly. The suggested method of excitation allows us to form steady standing waves of prescribed amplitude by simply fixing the driving frequency at any time, while the autoresonant driving compensates the effect of dissipation. We had also discussed and illustrated in simulations formation of autoresonant standing waves when replacing the microwave drive by a spatially modulated transverse spin torque driving or adding a modulated hard axis anisotropy. Developing a full Whitham's type theory in these cases and inclusion of dissipation and thermal fluctuations in the theory seem to be important goals for future research. Finally, it is known that the undriven, dissipationless LLG problem (1) is integrable [9]. This means that there exist many additional, so-called multiphase solutions in this problem. Addressing the question of excitation and control of this multitude of solutions by chirped frequency perturbations seems to comprise another interesting goal for the future.

ACKNOWLEDGMENTS

The authors would like to thank J.M. Robbins and E.B. Sonin for stimulating discussions and important comments. This work was supported by the Israel Science Foundation Grant No. 30/14 and the Russian state program AAAA-A18-118020190095-4.

APPENDIX: QUANTUM TWO-LEVEL MODEL

We perform our numerical simulations to lowest significant order in λ and, therefore, approximate LLG Eq. (1) as

$$\frac{\partial\mathbf{m}}{\partial\tau} \approx \mathbf{h}\times\mathbf{m} + \lambda\mathbf{m}\times(\mathbf{h}\times\mathbf{m}) = \mathbf{h}'\times\mathbf{m}, \quad (A1)$$

where $\mathbf{h}' = \mathbf{h} - \lambda\mathbf{h}\times\mathbf{m}$. Our numerical scheme for studying the evolution governed by Eq. (A1) is based on the

equivalent quantum two-level system (idea originated by Feynman [38], and recently used in studying magnetization inversion in single domain nanoparticles [29,30]). We solve

$$i\frac{\partial A_1}{\partial \tau} = \frac{d_0}{2}A_1 + dA_2, \tag{A2}$$

$$i\frac{dA_2}{\partial \tau} = -\frac{d_0}{2}A_2 + d^*A_1, \tag{A3}$$

where $A_{1,2} = A_{1,2}(\xi, \tau)$ are the wave functions of a pair of coupled quantum levels and

$$d_0 = h_z', \tag{A4}$$

$$d = \frac{(h_x' - ih_y')}{2}. \tag{A5}$$

The magnetization $\mathbf{m}$ in d_0 and d in Eqs. (A2), (A3) is related to $A_{1,2}$ via

$$\begin{aligned} m_x &= A_1A_2^* + A_1^*A_2 = 2B_1B_2\cos\varphi, \\ m_y &= i(A_1A_2^* - A_1^*A_2) = 2B_1B_2\sin\varphi, \\ m_z &= |A_1|^2 - |A_2|^2 = B_1^2 - B_2^2, \end{aligned} \tag{A6}$$

where $A_{1,2} = B_{1,2}\exp(i\varphi_{1,2})$ and $\varphi = \varphi_2 - \varphi_1$. Note that, as expected, the total population of our two level system remains constant, $|A_1|^2 + |A_2|^2 = |\mathbf{m}| = 1$. Note also that $m_\perp = \sqrt{m_x^2 + m_y^2} = 2B_1B_2$, while φ is the azimuthal rotation angle of the magnetization around ξ. Formally, the system (A2), (A3) comprises a set of two coupled NLS-type equations for wave functions $A_{1,2}$. The numerical approach to solving this system throughout this work used a standard pseudospectral method [43] subject to given initial and periodic boundary conditions.

[1] M. M. Scott, M. P. Kostylev, B. A. Kalinikos, and C. E. Patton, Phys. Rev. B **71**, 174440 (2005).
[2] M. Wu, M. A. Kraemer, M. M. Scott, C. E. Patton, and B. A. Kalinikos, Phys. Rev. B **70**, 054402 (2004).
[3] M. Wu, P. Krivosik, B. A. Kalinikos, and C. E. Patton, Phys. Rev. Lett. **96**, 227202 (2006).
[4] M. Chen, M. A. Tsankov, J. M. Nash, and C. E. Patton, Phys. Rev. Lett. **70**, 1707 (1993).
[5] A. Scott, *Nonlinear Science* (Oxford University Press, New York, 1999), p. 279.
[6] H. B. Braun, Adv. Phys. **61**, 1 (2012).
[7] G. Garbou, Math. Models. Meth. Appl. Sci. **11**, 1529 (2001).
[8] R. V. Kohn and V. Slastikov, Arch. Ration. Mech. Anal. **178**, 227 (2005).
[9] A. M. Kosevich, B. A. Ivanov, and A. S. Kovalev, Phys. Rep. **194**, 117 (1990).
[10] H.-J. Mikeska and M. Steiner, Adv. Phys. **40**, 191 (1991).
[11] G. S. D. Beach, C. Nistor, C. Knutson, M. Tsoi, and J. L. Erskine, Nat. Mater. **4**, 741 (2005).
[12] A. Goussev, R. G. Lund, J. M. Robbins, V. Slastikov, and C. Sonnenberg, Phys. Rev. B **88**, 024425 (2013).
[13] M. Negoita, T. J. Hayward, J. A. Miller, and D. A. Allwood, J. Appl. Phys. **114**, 013904 (2013).
[14] M. Sitte, K. Everschor-Sitte, T. Valet, D. R. Rodrigues, J. Sinova, and Ar. Abanov, Phys. Rev. B **94**, 064422 (2016).
[15] W. Wang, Z. Zhang, R. A. Pepper, C. Mu, Y. Zhou, and H. Fangohr, J. Phys.: Condens. Matter **30**, 015801 (2018).
[16] R. P. Cowburn, Nature (London) **448**, 544 (2007).
[17] L. Thomas, R. Moriya, C. Rettner, and S. S. P. Parkin, Science **330**, 1810 (2010).
[18] A. M. Kosevich, V. V. Gann, A. I. Zhukov, and V. P. Voronov, Zh. Eksp. Teor. Fiz. **114**, 735 (1998) [J. Exp. Theor. Phys. **87**, 401 (1998)].
[19] P. B. He and W. M. Liu, Phys. Rev. B **72**, 064410 (2005).
[20] Z.-D. Li, Q.-Y. Li, L. Li, and W. M. Liu, Phys. Rev. E **76**, 026605 (2007).
[21] E. M. McMillan, Phys. Rev. **68**, 143 (1945).
[22] V. I. Veksler, J. Phys. USSR **9**, 153 (1945).
[23] R. Malhotra, Nature (London) **365**, 819 (1993).
[24] L. Friedland, Astroph. J. Lett. **547**, L75 (2001).
[25] B. Meerson and L. Friedland, Phys. Rev. A **41**, 5233 (1990).
[26] H. Maeda, J. Nunkaew, and T. F. Gallagher, Phys. Rev. A **75**, 053417 (2007).
[27] J. Fajans, E. Gilson, and L. Friedland, Phys. Plasmas **6**, 4497 (1999).
[28] G. Klughertz, P.-A. Hervieux, and G. Manfredi, J. Phys. D: Appl. Phys. **47**, 345004 (2014).
[29] G. Klughertz, L. Friedland, P.-A. Hervieux, and G. Manfredi, Phys. Rev. B **91**, 104433 (2015).
[30] G. Klughertz, L. Friedland, P.-A. Hervieux, and G. Manfredi, J. Phys. D **50**, 415002 (2017).
[31] L. Friedland and A. G. Shagalov, Phys. Rev. Lett. **81**, 4357 (1998).
[32] M. A. Borich, A. G. Shagalov, and L. Friedland, Phys. Rev. E **91**, 012913 (2015).
[33] L. Friedland and A. G. Shagalov, Phys. Rev. E **71**, 036206 (2005).
[34] S. V. Batalov and A. G. Shagalov, Phys. Metals Metallog. **109**, 3 (2010).
[35] S. V. Batalov and A. G. Shagalov, Phys. Rev. E **84**, 016603 (2011).
[36] G. B. Whitham, *Linear and Nonlinear Waves* (Wiley, New York, 1974).
[37] L. Friedland, Scholarpedia **4**, 5473 (2009).
[38] R. Feynman, F. L. Vernon, and R. W. Hellwarth, J. Appl. Phys. **28**, 49 (1957).
[39] J. Fajans, E. Gilson, and L. Friedland, Phys. Plasmas **8**, 423 (2001).
[40] L. Friedland, Phys. Rev. E **58**, 3865 (1998).
[41] D. Backes, F. Macia, S. Bonetti, R. Kukreja, H. Ohldag, and A. D. Kent, Phys. Rev. Lett. **115**, 127205 (2015).
[42] J. Briones, F. Montaigne, D. Lacour, G. Lengaigne, S. Girod, and M. Hehn, Appl. Phys. Express **3**, 073002 (2010).
[43] C. Canuto, M. Y. Hussaini, A. Quarteroni, and T. A. Zang, *Spectral Methods in Fluid Dynamics* (Springer-Verlag, New York, 1988).